Article

Effect of Electron-Donating and Electron-Withdrawing Groups on Peptide/Single-Walled Carbon Nanotube Interactions

Vasiliki Z. Poenitzsch, David C. Winters, Hui Xie, Gregg R. Dieckmann, Alan B. Dalton, and Inga H. Musselman

J. Am. Chem. Soc., **2007**, 129 (47), 14724-14732 • DOI: 10.1021/ja0750827

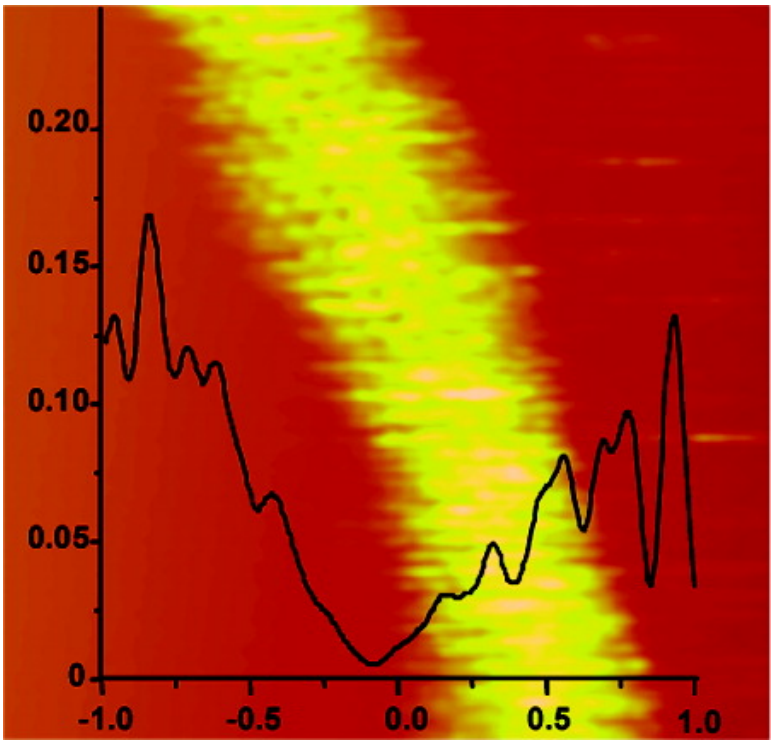

More About This Article

Additional resources and features associated with this article are available within the HTML version:

- Supporting Information
- Links to the 1 articles that cite this article, as of the time of this article download
- Access to high resolution figures
- Links to articles and content related to this article
- Copyright permission to reproduce figures and/or text from this article

J|A|C|S
ARTICLES
Published on Web 11/07/2007

Effect of Electron-Donating and Electron-Withdrawing Groups on Peptide/Single-Walled Carbon Nanotube Interactions

Vasiliki Z. Poenitzsch,[†] David C. Winters,[†] Hui Xie,[‡] Gregg R. Dieckmann,[†,‡] Alan B. Dalton,[§] and Inga H. Musselman*[,†,‡]

Contribution from the Department of Chemistry and the Alan G. MacDiarmid NanoTech Institute, The University of Texas at Dallas, 800 West Campbell Road, Richardson, Texas 75080, and the Department of Physics, University of Surrey, Guildford GU2 7XH, U.K.

Received July 9, 2007; E-mail: imusselm@utdallas.edu

Abstract: Nano-1, a designed peptide, has been demonstrated to efficiently disperse individual single-walled carbon nanotubes (SWNTs) by folding into an amphiphilic α-helix wherein the phenylalanine (Phe) residues on the hydrophobic face of the helix interact via π-stacking with the aromatic surface of the SWNT. In this study, the ability of electron-donating (hydroxyl) and electron-withdrawing (nitro) groups on the phenyl ring of Phe to affect the interactions between the peptide and SWNTs is examined by substituting the Phe residues in the nano-1 sequence with tyrosine and *p*-nitro-phenylalanine, respectively. Atomic force microscopy measurements and optical absorption spectroscopy revealed that the ability to disperse individual SWNTs increases with increasing electron density of the aromatic residue on the hydrophobic face of the amphiphilic helical peptides. Scanning tunneling spectroscopy (STS) and Raman analyses were used to examine the effect of noncovalent protein functionalization on the electronic properties of SWNTs. Small shifts in the Raman G band peak for the peptide/SWNT composites, as well as weak features that appear near the Fermi energy (E_f) in the STS d*I*/d*V* spectra of the peptide-coated SWNTs, are suggestive of a weak charge-transfer interaction between the peptides and the SWNTs.

The unique electronic properties of single-walled carbon nanotubes (SWNTs) are a major reason for interest in this material. Depending only on their diameter and chirality, SWNTs are either semiconducting or metallic.[1−4] Moreover, their nanometer diameters and micrometer lengths lead to large aspect ratios that make SWNTs behave as nearly ideal one-dimensional (1D) quantum wires.[3,4] Their high mechanical, thermal, and chemical stabilities further qualify SWNTs for use in nanoelectronic components.[5,6] However, it is widely recognized that the ability to tune the electronic properties of SWNTs into both n- and p-type materials is critical to their application in carbon-based nanoelectronics and to their ability to compete with current silicon-based microelectronic technology.[1,4] In addition, SWNTs have recently been considered as potential candidates for nanoelectronic devices and probes for biomedical diagnostic and clinical purposes.[7−11] Therefore, along with their electronic properties, the biocompatibility of SWNTs is another important factor for these applications.

Theoretical and experimental studies have shown that SWNTs are capable of interacting strongly with both electron donors and electron acceptors.[5,6,12−19] One approach for tailoring the electronic properties of SWNTs has been to add dopants, such as boron (B) and nitrogen (N) atoms, to the lattice of carbon nanotubes.[5,6,12] Scanning tunneling spectroscopy (STS) results

[†] Department of Chemistry, The University of Texas at Dallas.
[‡] Alan G. MacDiarmid NanoTech Institute, The University of Texas at Dallas.
[§] University of Surrey.

(1) Avouris, P. *Acc. Chem. Res.* **2002**, *35*, 1025−1034.
(2) Wildöer, J. W. G.; Venema, L. C.; Rinzler, A. G.; Smalley, R. E.; Dekker, C. *Nature* **1998**, *391*, 59−62.
(3) Odom, T. W.; Huang, J.-L.; Kim, P.; Lieber, C. M. *Nature* **1998**, *391*, 62−64.
(4) Shim, M.; Javey, A.; Kim, N. W. S.; Dai, H. *J. Am. Chem. Soc.* **2001**, *123*, 11512−11513.
(5) Carroll, D. L.; Redlich, Ph.; Blase, X.; Charlier, J.-C.; Curran, S.; Ajayan, P. M.; Rühle, M. *Phys. Rev. Lett.* **1998**, *81*, 2332−2335.
(6) Terrones, M.; Jorio, A.; Endo, M.; Rao, A. M.; Kim, Y. A.; Hayashi, T.; Terrones, H.; Charlier, J.-C.; Dresselhaus, G.; Dresselhaus, M. S. *Mater. Today* **2004**, *7*, 30−45.
(7) Tasis, D.; Tagmatarchis, N.; Bianco, A.; Prato, M. *Chem. Rev.* **2006**, *106*, 1105−1136.
(8) Bianco, A.; Kostarelos, K.; Partidos, C. D.; Prato, M. *Chem. Commun.* **2005**, *5*, 571−577.
(9) Ziegler, K. J. *Trends Biotechnol.* **2005**, *23* (9), 440−444.
(10) Barone, P. W.; Baik, S.; Heller, D. A.; Strano, M. *Nat. Mater.* **2005**, *4* (1), 86−92.
(11) Jeng, E. S.; Moll, A. E.; Roy, A. C.; Gastala, J. B.; Strano, M. S. *Nano Lett.* **2006**, *6* (3), 371−375.
(12) Czerw, R.; Terrones, M.; Charlier, J.-C.; Blase, X.; Foley, B.; Kamalakaran, R.; Grobert, N.; Terrones, H.; Tekleab, D.; Ajayan, P. M.; Blau, W.; Rühle, M.; Caroll, D. L. *Nano Lett.* **2001**, *1* (9), 457−460.
(13) Rao, A. M.; Eklund, P. C.; Bandow, S.; Thess, A.; Smalley, R. A. *Nature* **1997**, *388*, 257−259.
(14) Claye, A.; Rahman, S.; Fischer, J. E.; Sirenko, A.; Sumanasekera, G. U.; Eklund, P. C. *Chem. Phys. Lett.* **2001**, *333*, 16−22.
(15) Bendiab, N.; Anglaret, E.; Bantignies, J.-L.; Zahab, A.; Sauvajol, J. L.; Petit, P.; Mathis, C.; Lefrant, S. *Phys. Rev. B* **2001**, *64*, 245424-1−245424-6.
(16) Kong, J.; Franklin, N. R.; Zhou, C.; Chapline, M. G.; Peng, S.; Cho, K.; Dai, H. *Science* **2000**, *287*, 622−625.
(17) Collins, P. G.; Bradley, K.; Ishigami, M.; Zettl, A. *Science* **2000**, *287*, 1801−1804.
(18) Boul, P. J.; Liu, J.; Mickelson, E. T.; Huffman, C. B.; Ericson, L. M.; Chiang, I. W.; Smith, K. A.; Colbert, D. T.; Hauge, R. H.; Magrave, J. L.; Smalley, R. E. *Chem. Phys. Lett.* **1999**, *310*, 367−372.
(19) Tasis, D.; Tagmatarchis, N.; Georgakilas, V.; Prato, M. *Chem. Eur. J.* **2003**, *9*, 4000−4008.

10.1021/ja0750827 CCC: $37.00

and calculated local density of states (DOS) revealed that B-doped SWNTs exhibit strong electronic acceptor states in the valence band,[5] whereas N-doped SWNTs present electronic donor states in the conduction band.[6] Other studies have used ion doping focusing on alkali metals (e.g., potassium, rubidium, lithium) as donors and halogens (e.g., bromine, iodine) as acceptors.[13−15] In these studies, shifts in the characteristic SWNT Raman vibrational modes provided evidence for charge transfer between these dopants and the SWNTs.[13−15]

The electronic properties of SWNTs were also shown to be sensitive to the chemical environment wherein exposure to oxidizing gases (e.g., O_2, NO_2) increased electrical conductivity, whereas a reducing gas (NH_3) did the reverse.[16,17] STS measurements of SWNTs exposed to O_2 revealed a p-type behavior with a reduction of the apparent band gap and an increased density of valence band states.[17] Additionally, as-produced SWNTs have been found to be p-type, presumably due to an oxygen layer on the nanotube lattice.[20] This sensitivity of SWNT electronic properties to gases launched the prospect of introducing donor or acceptor levels through molecular adsorption. In one study, aromatic acceptor molecules (anthracene derivatives) were shown to strongly adsorb to SWNTs through a charge-transfer interaction, in which the SWNT acted as an electron donor and anthracene served as an acceptor.[21] In addition, doping of SWNTs by the adsorption of polymers with donor or acceptor functional groups has been reported.[4,22] Interestingly, a study comparing polyimide with a nitrile-functionalized polyimide revealed that a donor−acceptor interaction between SWNTs and the electron accepting nitrile-functionalized polymer resulted in improved SWNT dispersion.[22]

Interest in exploiting the remarkable properties of SWNTs in novel electrical devices is tempered by their hydrophobicity and tendency to aggregate into bundles or ropes due to intertube van der Waals forces. Since many applications will require the separation and further manipulation of SWNTs, substantial effort has been placed on developing techniques first to isolate individual SWNTs and then to assemble them into useful structures. One strategy for improving the dispersion of SWNTs is to functionalize them covalently at the side-wall.[18,19,23] Alternatively, SWNTs can be functionalized noncovalently by immobilizing aromatic molecules through π-stacking interactions[24] or disrupting the hydrophobic interface by wrapping SWNTs with a wide variety of molecules including surfactants,[25,26] conjugated polymers,[27−29] oligosaccharides,[30] and biological molecules.[31−33]

However, changes to the electronic structure of SWNTs through covalent or noncovalent functionalization are of fundamental importance to potential SWNT-based molecular devices and sensors. Covalently functionalized sites on the SWNT disrupt the extended π-network of sp^2 hybridized carbon atoms by introducing sp^3 hybridized carbons, which function as defects. Previous studies have shown that this change to the electronic structure of the SWNT simultaneously weakens all interband transitions and eventually destroys the electronic band structure altogether.[18,34,35] Additionally, side-wall covalent chemistry on metallic SWNTs has been shown to rapidly modulate the density of states at the Fermi energy (E_f), converting a metallic SWNT to a semiconducting SWNT.[35] Hence, one of the major advantages of noncovalent functionalization is the possibility of introducing chemical moieties for targets of interest without significantly perturbing the π-system and electronic structure of the SWNT.

Biological materials, such as peptides, are well-known in nature for having extreme specificity for other biomolecules or ligands and the ability to self-assemble into a wide variety of complex functional structures. In previous studies, we have demonstrated that a designed peptide, denoted nano-1, coats and debundles SWNTs and promotes the assembly of these coated nanotubes into novel hierarchical structures.[36−38] Nano-1 folds into an amphiphilic α-helix, in which apolar residues occupy one face of the helix and more polar residues form the other face. Amphiphilicity is achieved through appropriate placement of apolar and polar residues in the peptide primary sequence.[36] Importantly, the apolar face of nano-1 contains four phenylalanine (Phe) residues. Phe, being aromatic, should interact effectively with the SWNT surface via π-stacking.[36,37] In fact, results from a study involving a designed series of peptides based on the nano-1 sequence, in which the aromatic content was systematically varied, confirmed that π-stacking plays an important role in peptide/SWNT interactions.[38] In this context, π-stacking refers to the attractive interaction between two aromatic systems, here the phenylalanine in the peptide with the SWNT surface, that is predominantly due to dispersion forces.[39] Designed synthetic peptides may provide a route for tailoring the electronic properties of SWNTs, wherein the SWNT could potentially be doped by introducing electron donor or acceptor functional groups on the benzene ring of Phe. In this study, we will probe the effect of an electron-donating (hydroxyl) and an electron-withdrawing (nitro) group on peptide/SWNT interactions by substituting the Phe residues in the

(20) Sumanasekera, G. U.; Adu, C. K. W.; Fang, S.; Eklund, P. C. *Phys. Rev. Lett.* **2000**, *85* (5), 1096−1099.
(21) Zhang, J.; Lee, J.-K.; Wu, Y.; Murray, R. W. *Nano Lett.* **2003**, *3* (3), 403−407.
(22) Wise, K. E.; Park, C.; Siochi, E. J.; Harrison, J. S. *Chem. Phys. Lett.* **2004**, *391*, 207−211.
(23) Banerjee, S.; Hemraj-Benny, T.; Wong, S. S. *Adv. Mater.* **2005**, *17*, 17−29.
(24) Chen, R. J.; Zhang, Y.; Wang, D.; Dai, H. *J. Am. Chem. Soc.* **2001**, *123*, 3838−3839.
(25) Liu, J.; Rinzler, A. G.; Dai, H.; Hafner, J. H.; Bradley, R. K.; Boul, P. J.; Lu, A.; Iverson, T.; Shelimov, K.; Huffman, C. B.; Rodriguez-Macias, F.; Shon, Y.-S.; Lee, T. R.; Colbert, D. T.; Smalley, R. E. *Science* **1998**, *280*, 1253−1256.
(26) Islam, M. F.; Rojas, E.; Bergey, D. M.; Johnson, A. T.; Yodh, A. G. *Nano Lett.* **2003**, *3*, 269−273.
(27) Dalton, A. B.; Stephan, C.; Coleman, J. N.; McCarthy, B.; Ajayan, P. M.; Lefrant, S.; Bernier, P.; Blau, W. J.; Byrne, H. J. *J. Phys. Chem. B* **2000**, *104*, 10012−10016.
(28) Carillo, A.; Swartz, J. A.; Gamba, J. M.; Kane, R. S. *Nano Lett.* **2003**, *3*, 1437−1440.
(29) Chambers, G.; Carroll, C.; Farrell, G. F.; Dalton, A. B.; McNamara, M.; in het Panhuis, M.; Byrne, H. J. *Nano Lett.* **2003**, *3*, 843−846.
(30) Star, A.; Steuerman, D. W.; Heath, J. R.; Stoddart, J. F. *Angew. Chem., Int. Ed.* **2002**, *41*, 2508−2512.
(31) Wang, S.; Humphreys, E. S.; Chung, S.-Y.; Delduco, D. F.; Lustig, S. R.; Wang, H.; Parker, K. N.; Rizzo, N. W.; Subramoney, S.; Chiang, Y.-M.; Jagota, A. *Nat. Mater.* **2003**, *2*, 196−200.
(32) Zheng, M.; Jagota, A.; Semke, E. D.; Diner, B. A.; McLean, R. S.; Lustig, S. R.; Richardson, R. E.; Tassi, N. G. *Nat. Mater.* **2003**, *2*, 338−342.
(33) Lin, Y.; Allard, L. F.; Sun, Y.-P. *J. Phys. Chem. B* **2004**, *108*, 3760−3764.
(34) Chen, J.; Hamon, M. A.; Hu, H.; Chen, Y.; Rao, A. M.; Eklund, C.; Haddon, R. C. *Science* **1998**, *282*, 95−98.
(35) Kamaras, K.; Itkis, M. E.; Hu, H.; Zhao, B.; Haddon, R. C. *Science* **2003**, *301*, 1501.
(36) Dieckmann, G. R.; Dalton, A. B.; Johnson, P. A.; Razal, J.; Chen, J.; Giordano, G. M.; Muñoz, E.; Musselman, I. H.; Baughman, R.; Draper, R. K. *J. Am. Chem. Soc.* **2003**, *125*, 1770−1777.
(37) Zorbas, V.; Ortiz-Acevedo, A.; Dalton, A. B.; Yoshida, M. M.; Dieckmann, G. R.; Draper, R. K.; Baughman, R. H.; Yacaman, M. J.; Musselman, I. H. *J. Am. Chem. Soc.* **2004**, *126*, 7222−7226.
(38) Zorbas, V.; Smith, A. L.; Hie, X.; Ortiz-Acevedo, A.; Dalton, A. B.; Dieckmann, G. R.; Draper, R. K.; Baughman, R. H.; Musselman, I. H. *J. Am. Chem. Soc.* **2005**, *127*, 12323−12328.
(39) Wang, Y. L.; Mao, L. S.; Hu, X. C. *Biophys. J.* **2004**, *86*, 3097−3111.

Table 1. Amphiphilic Helical Peptides Designed to Test the Role of Electron-Donating and Electron-Withdrawing Groups on Peptide/SWNT Interactions[a]

nano-1	E VEAFEKK VAAFESK VQAFEKK VEAFEHG
Tyr-nano-1	E VEAYEKK VAAYESK VQAYEKK VEAYEHG
nitro-nano-1	E VEAF*EKK VAAF*ESK VQAF*EKK VEAF*EHG

[a] Seven-residue repeats indicate helix heptads. The effect of an electron-donating (hydroxyl) or an electron-withdrawing (nitro) group was examined by substituting the phenylalanine (F) residues in the nano-1 sequence with tyrosine (Y) and *p*-nitro-phenylalanine (F*), respectively.

nano-1 sequence with tyrosine and *p*-nitro-phenylalanine, respectively (Table 1). These specific substituents were chosen on the basis of their Hammett-σ values, a measure of electronegativity defined on the basis of the ionization constant of a substituted benzoic acid in water (Supporting Information). The effect of the noncovalent protein functionalization on the electronic properties of SWNTs will also be examined using Raman and STS analyses.

Experimental Section

Peptide Synthesis and Purification. The peptides nano-1, Tyr-nano-1, and nitro-nano-1 (Table 1) were synthesized and purified following previously published methods.[36−38,40]

Peptide/SWNT Sample Preparations. Solutions of 20 μM and 100 μM nitro-nano-1 were prepared using deionized water, and the peptide concentration was verified using quantitative amino acid analysis (analysis done by the Iowa State Protein Facility). The nitro-nano-1 extinction coefficient was then determined by preparing a Beer's Law standard calibration curve (Supporting Information). Solutions of 100 μM nano-1 and 100 μM Tyr-nano-1 peptides were prepared using deionized water. Peptide concentrations were verified using UV molecular absorption spectrometry, with the peptide extinction coefficients calculated based on the extinction coefficients of the chromophores, Phe and Tyr (197 L mol^{-1} cm^{-1} at 257 nm and 1420 L mol^{-1} cm^{-1} at 276 nm), respectively.

SWNTs produced by high-pressure decomposition of carbon monoxide (HiPco process)[41] were supplied by Carbon Nanotechnologies, Inc. (lot no. R0233). For each sample, a 1 mL volume of 20 μM or 100 μM peptide was added to HiPco SWNTs (0.75−1.50 mg) in an Eppendorf tube, and the mixture was then vortexed for approximately 1 min. Peptide/SWNT samples were then sonicated for 1 min with the sample immersed in an ice water bath using a VWR Scientific Branson Sonifier 250 at a power level of 10 W, yielding dense black mixtures. The sonicated samples were centrifuged for 10 min at 700*g* in an Eppendorf 5417C centrifuge. The upper 75% of the supernatant was recovered using a small-bore pipet and transferred to a Beckman centrifuge tube. Samples were then centrifuged for 30 min at 50 000*g* in a Beckman TL-100 ultracentrifuge with the temperature controlled at 4 °C. The upper 50% of the supernatant was recovered using a small-bore pipet, avoiding sediment at the bottom, and transferred to a clean tube. The 50 000*g* supernatants were diluted 10-fold with deionized water, and 10 μL volumes were drop-cast onto freshly cleaved muscovite mica (Asheville-Schoonmaker Mica Co.) and allowed to dry for 24 h in a desiccator prior to imaging by AFM. Aliquots (20 μL) of the same supernatants were also spun-cast onto Au(111)-coated mica (Molecular Imaging) for imaging by STM. Peptide control samples, lacking SWNTs, were prepared using an identical procedure.

Atomic Force Microscopy (AFM). AFM images of sample preparations were obtained using a Digital Instruments, Inc. Nanoscope III Multimode Scanning Probe microscope operated in tapping mode. Silicon cantilevers/tips (Veeco Probes) with force constants of 5.0 N m^{-1} and an average resonant frequency of 180 kHz were used to ensure minimal sample compression.[42] The AFM J scanner was calibrated using a NanoDevices Inc. standard consisting of lines with 2 μm pitch and 20 nm height, dimensions similar to those of SWNTs. The height calibration was verified using hydrofluoric acid etched pits in muscovite mica where 2 nm steps are observed along the long axis and 1 nm steps are observed along the short axis.[43] SWNT diameters were determined using AFM height measurements. AFM image acquisition parameters for height analysis of peptide-coated SWNTs included a scan size of 2.0 × 2.0 μm^2 and a reduced *Z*-limit range (100−200 V).[42] Images were acquired from at least three different areas on each substrate to ensure that the data were representative of the sample.

Scanning Tunneling Microscopy (STM) and Scanning Tunneling Spectroscopy (STS). STM images were acquired using a Digital Instruments, Inc. Nanoscope III STM with a 0.7 μm A scanner and commercial Pt/Ir tips (Veeco Probes) operated at room temperature and ambient conditions. Typical image acquisition parameters included current set points of 400−600 pA and bias voltages of 600−800 mV. The mechanical vibrations were isolated by setting the STM on a gel pad on a cement block attached to a tripod with bungee cords. The tip was engaged in the constant current mode with a large scan size ranging from 100−400 nm in order to ensure scanning on the surface of a Au-(111) island. After determining the presence of SWNTs, the scan size was reduced and the imaging conditions were changed to the constant height mode.

During brief interruptions in the STM scans, the microscope was switched to the STS mode of operation, and local $I-V$ curves were acquired on the same region of the SWNT as was imaged by STM. STS $I-V$ spectra were collected from −1.0 to 1.0 V. Before taking STS measurements, reference measurements were performed on the gold substrate to ensure the $I-V$ curves on gold were ohmic. In order to reduce noise, 20 $I-V$ curves were signal averaged and, after numerical differentiation, the resulting dI/dV curve was Fourier filtered. STS $I-V$ curves were also taken at approximately the same position on a bare SWNT spun-cast from a dispersion in 1,2-dichloroethane onto a Au(111)-coated mica substrate. STS dI/dV curves taken at the same position on the SWNT control showed consistent features demonstrating reliability in the measurements (Supporting Information).

Ultraviolet−Visible−Near-Infrared (UV−Vis−NIR) Spectrophotometry. Peptide/SWNT dispersions were prepared following the described sample preparation procedures using D_2O in place of deionized water. Absorption spectra of peptide/SWNT dispersions in D_2O were acquired using a common D_2O blank in a Perkin-Elmer Lambda 900 UV−vis−NIR spectrophotometer.

Circular Dichroism (CD) Spectroscopy. CD spectra were acquired at 25 °C using an Aviv model 202 circular dichroism spectrometer and a 1 mm path length rectangular quartz cuvette. Spectra were collected from 190 to 260 nm at 1 nm intervals using a 6 s dwell time at each wavelength increment.

Raman Spectroscopy. Peptide/SWNT supernatants (∼2 μL) were spotted on a SpectRim substrate (Tienta Sciences, Inc.) and placed in a desiccator to dry prior to Raman analysis. Raman analyses were acquired from three different peptide/SWNT sample preparations to ensure reproducibility. Raman spectra were taken using a Jobin Yvon Horiba high-resolution LabRam Raman microscope system, which has an optical microscope adapted to a double-grating spectrograph and a CCD array detector. A Spectra-Physics model 127 helium−neon laser provided the excitation at 632.8 nm. The laser power at the sample was ∼8 mW and was focused to a spot of ∼1 μm diameter using a 10× objective lens and 25 μm slit. Wavenumber calibration was carried

(40) Bodanzsky, M. *Peptide Chemistry: A Practical Approach*, 2 ed.; Springer-Verlag: New York 1993.
(41) Nikolaev, P.; Bronikowski, M.; Bradley, R.; Rohmund, F.; Colbert, D.; Smith, K.; Smalley, R. E. *Chem. Phys. Lett.* **1999**, *313*, 91−97.
(42) Poenitzsch, V. Z.; Musselman, I. H. *Microsc. Microanal.* **2006**, *12*, 221−227.
(43) Nagahara, L. A.; Hashimoto, K.; Fujishima, A. *J. Vac. Sci. Technol., B* **1994**, *12* (3), 1694−1697.

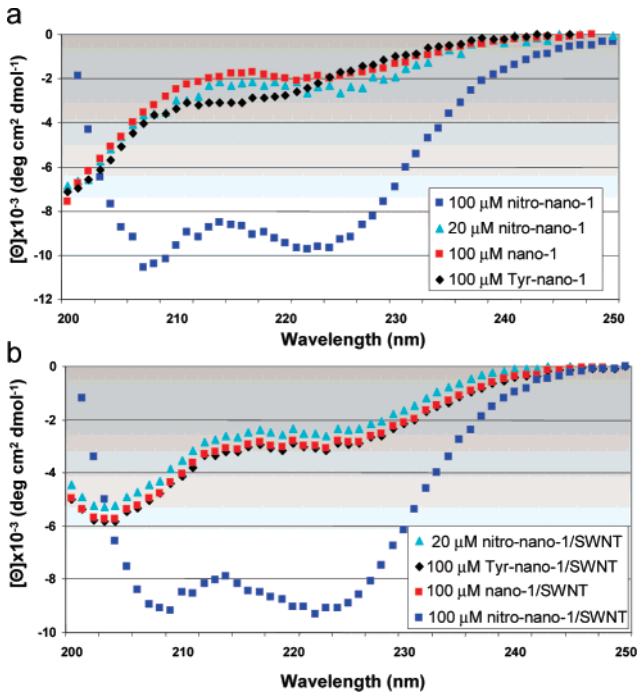

Figure 1. CD spectra of peptides (a) in water and (b) in water and in the presence of SWNTs: 100 μM nano-1, 100 μM Tyr-nano-1, 100 μM nitro-nano-1, and 20 μM nitro-nano-1.

out using the 520.5 cm^{-1} line of the silicon wafer. Spectra were recorded by scanning the 50−3000 cm^{-1} region with a total acquisition time of 5 min. Spectra were fitted with Lorentzian functions by searching for the minimum number of frequencies that fit the different bands equally well without fixing the positions and widths of the individual peaks.

Results and Discussion

In this study, the effect of an electron-donating (hydroxyl) group and an electron-withdrawing (nitro) group on peptide/SWNT interactions is examined by substituting the Phe residues in the nano-1 sequence with tyrosine and *p*-nitro-phenylalanine, respectively (Table 1). Besides electron-donating and electron-withdrawing character, another variable among the peptides that could affect their interactions with SWNTs is secondary structure. Consequently, CD was utilized to characterize the peptide's ability to fold in aqueous solution, both alone and in the presence of SWNTs. Figure 1a shows the CD spectra of the peptides (100 μM nano-1, 100 μM Tyr-nano-1, 100 μM nitro-nano-1, and 20 μM nitro-nano-1) in water. At approximately pH 6 and 25 °C, 100 μM nitro-nano-1 exhibits prominent negative CD peaks at 222 and 208 nm indicative of α-helical secondary structure, whereas 100 μM solutions of nano-1 and Tyr-nano-1 display significantly less helical and more random coil secondary structure. Amphiphilic peptides with a significant degree of α-helical structure in aqueous solution most likely self-associate to a greater degree (larger K_{Assoc}) and, thereby, should be less effective at dispersing SWNTs. However, at 20 μM the CD spectrum of nitro-nano-1 closely resembles those of 100 μM nano-1 and 100 μM Tyr-nano-1, indicating a similar degree of folding in aqueous solution and, conceivably, a comparable SWNT dispersal ability.

This optimal concentration of 20 μM for nitro-nano-1 was determined by acquiring CD spectra as a function of peptide concentration (Supporting Information). It is known for amphiphilic helical peptides that the CD spectra are dependent on peptide concentration, showing intensified helical signal with increasing concentration.[44] This behavior, which is indicative of an associating system, is indeed observed for all of the peptides in this study.[36] Nano-1 and Tyr-nano-1 appear to form helical aggregates in solution at higher concentrations compared to nitro-nano-1. Altogether, these results suggest that, compared to nano-1 and Tyr-nano-1, nitro-nano-1 more effectively self-assembles to form helical aggregates in solution.

The CD spectra of 100 μM nano-1, 100 μM Tyr-nano-1, and 20 μM nitro-nano-1 in the presence of SWNTs (Figure 1b) displayed more prominent signals at 208 and 222 nm compared to spectra of the peptides alone (Figure 1a). This result reveals that these peptides adopt a higher degree of α-helical structure in aqueous solution as a result of stabilization by hydrophobic interactions between the peptide *a*/*d* face and the SWNT surface. This behavior is identical to that previously reported for nano-1.[36] More importantly, the CD spectra of 100 μM nano-1/SWNT, 100 μM Tyr-nano-1/SWNT, and 20 μM nitro-nano-1/SWNT dispersions match very closely, suggesting an analogous secondary structure. Thus, these three samples will enable us to examine the effect of the electron-donating/withdrawing character of a functional group on peptide/SWNT interactions in the absence of secondary structure effects.

The 20 μM nitro-nano-1/SWNT, 100 μM nano-1/SWNT, and 100 μM Tyr-nano-1/SWNT dispersions were all generated using an identical sample preparation procedure. Peptide/SWNT sample preparations were repeated at least three times for each peptide to ensure reproducibility. AFM images of 20 μM nitro-nano-1/SWNT, 100 μM nano-1/SWNT, and 100 μM Tyr-nano-1/SWNT dispersions (Figure 2) exhibited many individual peptide-coated SWNTs. In contrast, AFM images of the peptide control samples exhibited no SWNT-like features, demonstrating that the peptides alone do not form fibrillar structures (Supporting Information). AFM height measurements, which provide an accurate measure of SWNT diameter,[42] were obtained for the three peptide/SWNT dispersions. AFM height analysis of the 20 μM nitro-nano-1/SWNT dispersion ranged from 0.7 to 7.4 nm, with an average diameter of 2.6 ± 1.4 nm (four 2.0 × 2.0 μm^2 images, $n = 200$). Diameters of the 100 μM nano-1/SWNT dispersion ranged from 0.9 to 6.9 nm, with an average diameter of 2.4 ± 1.2 nm (four 2.0 × 2.0 μm^2 images, $n = 215$). Diameters of 100 μM Tyr-nano-1/SWNT dispersions provided a diameter distribution ranging from 0.8 to 9.8 nm, with an average diameter of 2.0 ± 1.3 nm (three 2.0 × 2.0 μm^2 images, $n = 200$). Considering the reported diameters of pristine HiPco SWNTs,[41] and the fact that the peptide coating can add an additional 1 to 3 nm, these height measurements for 100 μM Tyr-nano-1/SWNT, 100 μM nano-1/SWNT, and 20 μM nitro-nano-1/SWNT dispersions suggest that the majority of the observed nanotubes are individual SWNTs coated with peptide. Additionally, AFM images of nitro-nano-1/SWNT, nano-1/SWNT, and Tyr-nano-1/SWNT dispersions showed an increase in SWNT density with an increase in the donating character of the functional group substituted on the Phe residues of the peptide (Figure 2). AFM images of the 100 μM nitro-nano-1/SWNT samples exhibited minimal SWNT dispersion and the

(44) Lau, S. H.; Rivier, J.; Vale, W.; Kaiser, E. T.; Kézdy, F. J. *Proc. Natl. Acad. Sci. U.S.A.* **1983**, *80*, 7070−7074.

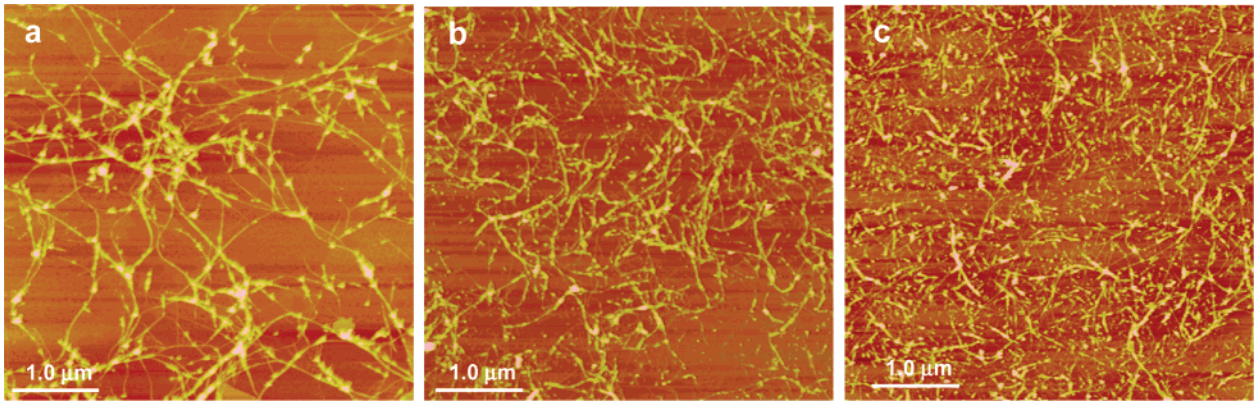

Figure 2. AFM images (5.0 × 5.0 μm^2) of (a) 20 μM nitro-nano-1/SWNT, (b) 100 μM nano-1/SWNT, and (c) 100 μM Tyr-nano-1/SWNT dispersions.

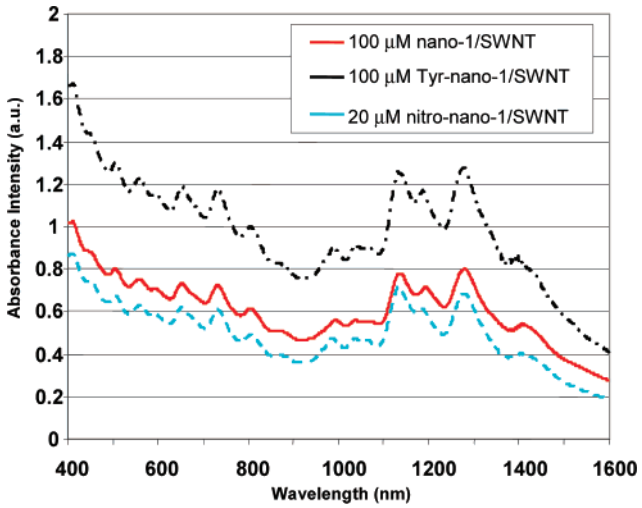

Figure 3. Absorption spectra of 100 μM nano-1/SWNT, 100 μM Tyr-nano-1/SWNT, and 20 μM nitro-nano-1/SWNT dispersions.

presence of predominantly uncoated SWNTs (Supporting Information). Likewise, UV−vis−NIR absorption spectra of the 100 μM nitro-nano-1/SWNT samples showed a decrease in SWNT dispersion compared to that of the 20 μM nitro-nano-1/SWNT samples (Supporting Information). These results suggest that, at higher peptide concentrations, nitro-nano-1 helices prefer to self-associate rather than interact with SWNTs.

The well-resolved spectral features in the UV−vis−NIR absorption spectra of the peptide/SWNT dispersions further suggest that the SWNTs are debundled in aqueous solution (Figure 3).[45] The absorption peaks of these spectra match closely in wavelength but differ in intensity. The increased intensity of the absorption spectra (20 μM nitro-nano-1/SWNT < 100 μM nano-1/SWNT < 100 μM Tyr-nano-1/SWNT) corroborates the AFM evidence of an increase in the amount of SWNTs dispersed with an increase in the electron density of the aromatic residue on the hydrophobic face of the amphiphilic helical peptides.

Raman spectroscopy was also used to probe the peptides' impact on the electronic structure of the SWNTs. Previous studies have demonstrated that the tangential vibrational modes for SWNTs are sensitive to doping.[13,15,27] Specifically, the G band peak was shown to shift to lower frequencies for electron donor dopants and to higher frequencies for electron acceptor dopants.[13,15,22] Additionally, a study of a semiconjugated organic polymer and SWNT hybrid system showed debundling of SWNTs by the polymer as another component that could contribute to Raman spectral shifts of SWNTs.[27] Figure 4a compares the tangential mode features for raw HiPco SWNTs and the nano-1/SWNT composite. Raman analyses were repeated three times with a mean upshift of 5.8 ± 0.4 cm^{-1} in

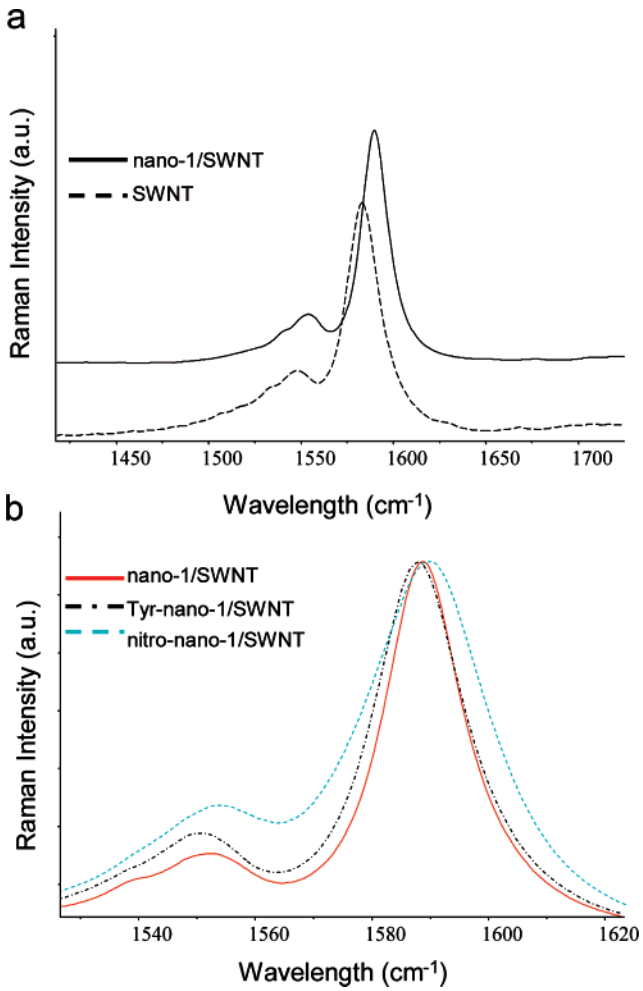

Figure 4. Raman spectra showing the tangential mode features for (a) raw HiPco SWNTs and 100 μM nano-1/SWNT composite and (b) 100 μM nano-1/SWNT, 100 μM Tyr-nano-1/SWNT, and 20 μM nitro-nano-1/SWNT dispersions.

(45) O'Connell, M. J.; Bachilo, S. M.; Huffman, C. B.; Moore, V. C.; Strano, M. S.; Haroz, E. H.; Rialon, K. L.; Boul, P. J.; Noon, W. H.; Kittrell, C.; Ma, J.; Hauge, R. H.; Weisman, R. B.; Smalley, R. E. *Science* **2002**, *297*, 593−596.

the G band of the nano-1/SWNT spectrum. This shift provides further support of nano-1's debundling ability as well as for charge transfer between the SWNTs. Figure 4b compares the tangential mode features for 100 μM nano-1/SWNT, 100 μM Tyr-nano-1/SWNT, and 20 μM nitro-nano-1/SWNT dispersions. The G band peak of all of these peptide/SWNT dispersions are upshifted with respect to that of uncoated HiPco SWNTs. However, compared to 100 μM nano-1/SWNT (red line), there is a slight downshift in the G band of 100 μM Tyr-nano-1/SWNT (black line) and, conversely, a slight upshift in the G band of 20 μM nitro-nano-1/SWNT (light blue line). The Raman analyses were repeated three times in order to determine that the observed shifts, while small, are real. The average peak downshift for the G band of the 100 μM Tyr-nano-1/SWNT dispersions was -0.6 ± 0.2 cm^{-1}, whereas the average peak upshift for the G band of the 20 μM nitro-nano-1/SWNT dispersions was 0.7 ± 0.3 cm^{-1}. The magnitude of these peak shifts is consistent with the minute change to the peptide design of adding one substituent to the benzene ring of Phe, which interacts via π-stacking with the nanotube wall. Moreover, the direction of the shifts correlates with the electron-donating and electron-withdrawing character of the substituent. These shifts supply evidence for a weak charge transfer between the SWNTs and the peptides.

To further examine the peptide's impact on the SWNT electronic properties, we used the spectroscopic capabilities of the STM. STS measurements were performed on peptide/SWNT dispersions as well as peptide and SWNT control samples spun-cast onto atomically flat Au(111)-coated mica substrates. Samples were first imaged by AFM to ensure reasonable SWNT distribution on the substrate as well as to confirm the predominance of individual peptide-coated SWNTs. The AFM images of 20 μM nitro-nano-1/SWNT, 100 μM nano-1/SWNT, and 100 μM Tyr-nano-1/SWNT dispersions confirmed a suitable density of individual peptide-coated SWNTs for further STM and STS analyses (Supporting Information). AFM images of the peptide control samples exhibited no SWNT-like features, demonstrating that the peptides alone do not form fibrillar structures (Supporting Information). Likewise, STM images of the peptide control samples exhibited no SWNT-like features (Supporting Information). STM images of SWNTs coated with nitro-nano-1, nano-1, and Tyr-nano-1 are shown for comparison with that of an uncoated SWNT in Figure 5. Overall, STM images of the three different peptide/SWNT composites are similar, exhibiting long tubular features coated with peptide. Peptides have little intrinsic conductivity, and therefore, no fine atomic structure can be readily resolved by STM. Yet, the STM images reveal an important detail about the peptide−SWNT interactions in that they show that all three peptides efficiently or fully coat the SWNTs.

STS $I-V$ curves were acquired from 11 bare SWNTs spun-cast from three different dispersions in 1,2-dichloroethane onto Au(111) as a control sample. The tunneling conductance (dI/dV vs bias voltage) is proportional to the local density of states (DOS) for metals and semiconductors.[46] The SWNT STS dI/dV curves are analogous to those reported in the literature for SWNTs.[3,4] A total of 73% or eight SWNTs exhibited a pronounced dip in the DOS in the vicinity of the Fermi level, typical of semiconducting tubes, whereas 27% or three SWNTs exhibited a nonzero DOS in the vicinity of the Fermi level, suggesting the presence of metallic tubes. At larger bias voltages away from the Fermi level, the STS dI/dV spectra exhibited relatively sharp, regularly spaced features, characteristic of van Hove singularities (VHS).

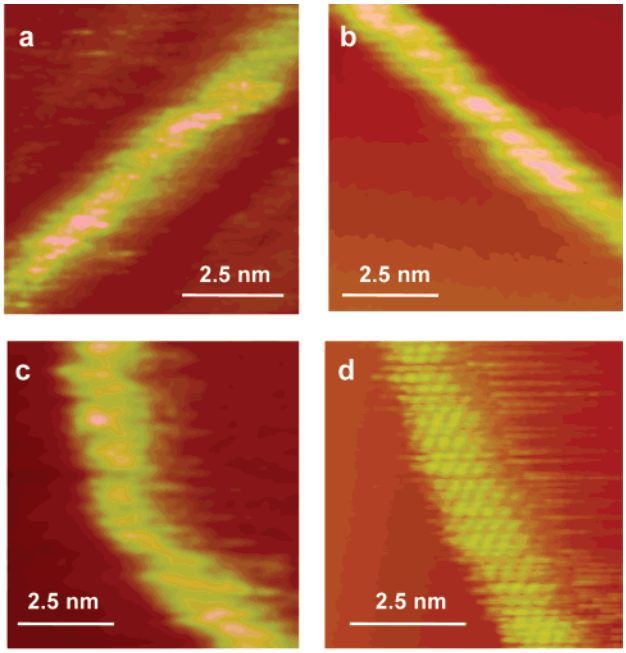

Figure 5. STM images (10.0 × 10.0 nm^2) of SWNTs coated with (a) 20 μM nitro-nano-1, (b) 100 μM nano-1, and (c) 100 μM Tyr-nano-1 compared with that of (d) an uncoated SWNT, demonstrating that the SWNTs are efficiently or fully coated with peptide.

Figure 6 compares the STS dI/dV spectrum of the nano-1 control sample on Au(111) with those of the nano-1/SWNT dispersion. The dominant contributions to the nano-1/SWNT DOS (Figure 6, parts b and c) must come from the SWNT because the peptide's DOS is comparatively featureless (Figure 6a, see also the Supporting Information). Moreover, the nano-1/SWNT dI/dV spectra also exhibit relatively sharp, regularly spaced features that are characteristic of VHS, originating from the one-dimensionality of SWNTs. STS spectra were acquired from 14 nano-1-coated SWNTs in multiple sample preparations, for which 12 displayed semiconducting behavior and 2 exhibited metallic behavior, corresponding to 86% and 14% of the tubes investigated, respectively. The dI/dV spectrum in Figure 6b shows a nearly vanishing DOS in the vicinity of the Fermi energy implying that this SWNT, coated with peptide, is electronically semiconducting. The other nano-1-coated SWNT (Figure 6c) has a nonvanishing DOS in the vicinity of the E_f, which is consistent with metallic behavior.

Figure 7a presents an STM image of a SWNT containing both uncoated and nano-1-coated regions. The uncoated SWNT area is distinguishable from the nano-1-coated portion by the atomic carbon lattice structure, more clearly observed in the higher resolution STM image of the same area provided in the inset (Figure 7a). STM images of SWNTs often do not show a hexagonal configuration of carbon atoms but, instead, exhibit a triangular lattice of dark and bright dots as shown in the inset of Figure 7a. The measured distance between two adjacent bright spots is 0.26 ± 0.01 nm, which correlates with the atomic spacing of carbon in the planar graphene lattice. The dI/dV spectra acquired from uncoated and nano-1-coated regions of

(46) Tersoff, J.; Hamann, D. R. *Phys. Rev. B* **1985**, *31*, 805−813.

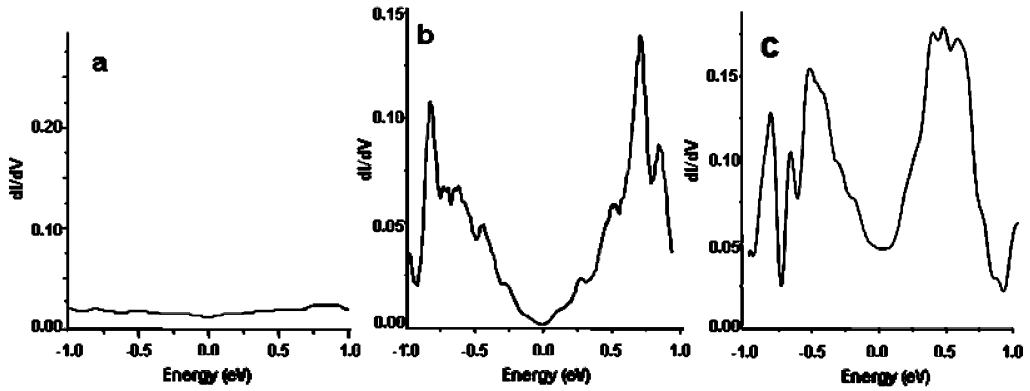

Figure 6. STS d*I*/d*V* spectra (DOS) of (a) nano-1 control sample on Au(111) and (b and c) nano-1-coated SWNTs on Au(111). The nano-1/SWNT d*I*/d*V* spectra exhibit VHS peaks, clearly originating from the 1D SWNTs, as the nano-1 DOS (a) is featureless. The nano-1/SWNT d*I*/d*V* spectra show both (b) a nearly vanishing DOS and (c) a nonvanishing DOS in the vicinity of the Fermi energy, suggesting that these two SWNTs coated with nano-1 are electronically semiconducting and metallic, respectively.

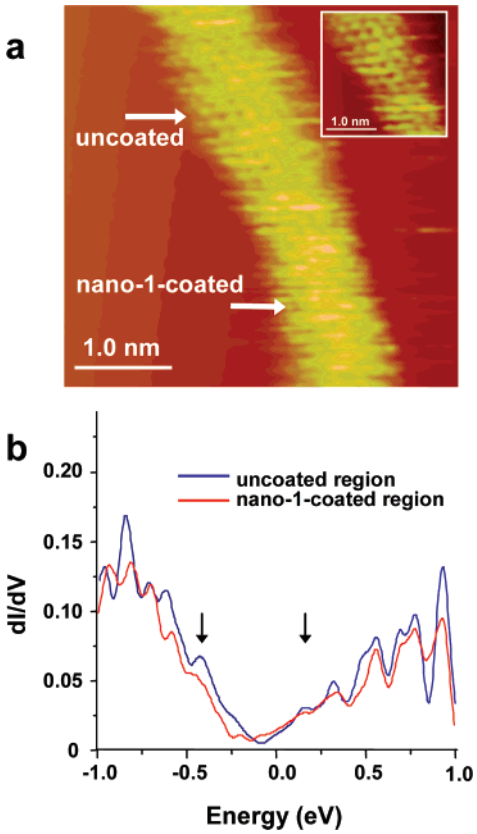

Figure 7. (a) STM image of a SWNT containing both uncoated and nano-1-coated regions. The inset is a higher resolution STM image of the same uncoated area more clearly depicting the atomic carbon lattice structure. (b) STS d*I*/d*V* spectra (DOS) acquired at positions along the uncoated and nano-1-coated regions of the SWNT. The DOS of the nano-1-coated portion of the SWNT closely resembles that of the uncoated region with some slight modifications.

the SWNT are compared in Figure 7b. The tunneling conductance along the bare SWNT (blue line, Figure 7b) exhibits the expected VHS peaks and a pronounced dip in the DOS in the vicinity of the Fermi energy, implying semiconducting behavior. In this DOS plot, the band gap is asymmetrically positioned around the zero bias voltage, shifted toward negative energy. This shift of the Fermi energy toward the valence band of the SWNT has been previously noted and ascribed to charge transfer or doping from the Au(111) substrate, which has a higher work function than the SWNTs.[47−49]

The d*I*/d*V* spectrum of the nano-1-coated portion (red line, Figure 7b) of the SWNT resembles that of the uncoated region with some modifications. At first glance, it would appear that the band gap in the peptide-coated SWNT DOS is shifted even further toward negative energy; however, at closer examination, it is evident that the energy positions of the first two VHS peaks are not strongly altered. The black arrows in Figure 7b identify what appears to be the first two VHS peaks in the uncoated SWNT DOS and, thus, approximately delineate the band gap region. Using these black arrows as a guide, it is clear that there is a very small, if any, shift in the energy positions of the first two VHS peaks in the DOS of the peptide-coated SWNT region. This minor shift could be due to either a slight doping of the SWNT by the peptide or, perhaps, a nonuniform doping by the substrate. Notably, these peaks are less sharp and slightly weaker than those in the DOS of the uncoated SWNT portion. Although there is generally an unavoidable broadening of VHS peaks in STS measurements, theoretical calculations also predict that the intertube interactions within a rope smooth out the spikelike structure of the singularities,[47] and experimental STS data of a conjugated polymer/SWNT composite exhibited broadening of VHS peaks.[50] Likewise, it is possible that the $\pi-\pi$ interactions between the peptide and SWNT could also result in similar broadening of VHS peaks.

Although the apparent band gap is relatively similar, there are differences in the DOS spectra in the vicinity of the Fermi energy for the nano-1-coated SWNT region compared to that of the uncoated section. Specifically, weak features appear in the negative portion, or on the valence band side, near the E_f at 0.09 and 0.20 eV. The position of the first two VHS peaks about the Fermi level, as well as VHS peaks in the positive portion or on the conduction band side in the d*I*/d*V* spectra, are analogous between the peptide-coated and uncoated regions. However, there are fluctuations in the VHS peak positions on the valence band side (negative portion) in the d*I*/d*V* spectrum of the peptide-coated region compared to that of the uncoated region. STS curves were taken at different positions ~10 nm apart along both the uncoated and peptide-coated regions

(47) Rubio, A. *Appl. Phys. A* **1999**, *68*, 275−282.
(48) Janssen, J. W.; Lemay, S. G.; Kouwenhoven, L. P.; Dekker, C. *Phys. Rev. B* **2002**, *65*, 115423-1−115423-5.
(49) LeRoy, B. J.; Lemay, S. G.; Kong, J.; Dekker, C. *Appl. Phys. Lett.* **2004**, *84* (21), 4280−4281.
(50) McCarthy, B.; Coleman, J. N.; Czerw, R.; Dalton, A. B.; Byrne, H. J.; Tekleab, D.; Iyer, P.; Ajayan, P. M.; Blau, W. J.; Carroll, D. L. *Nanotechnology* **2001**, *12* (3), 187−190.

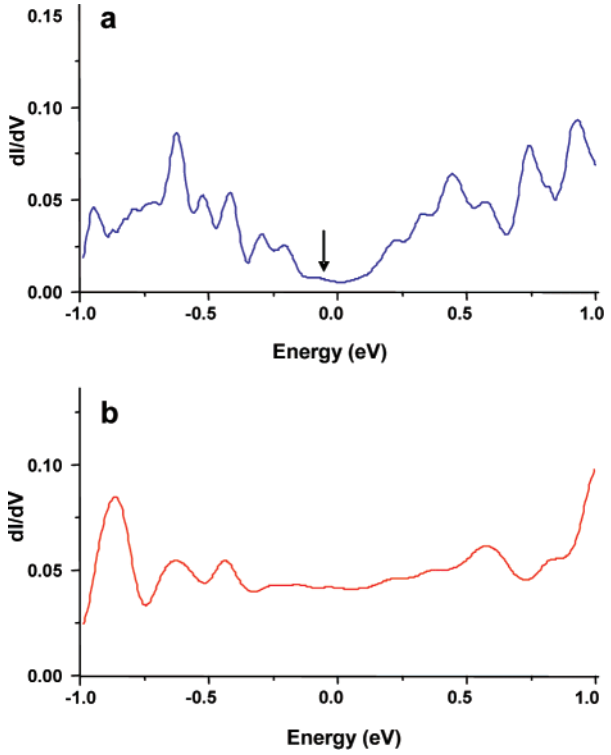

Figure 8. STS d*I*/d*V* curves of nitro-nano-1-coated SWNTs on Au(111) show both (a) a vanishing DOS and (b) a nonvanishing DOS in the vicinity of the Fermi energy, suggesting that these two SWNTs coated with nitro-nano-1 are electronically semiconducting and metallic, respectively. The black arrow in (a) points to a weak peak that appears on the valence band side near the Fermi energy.

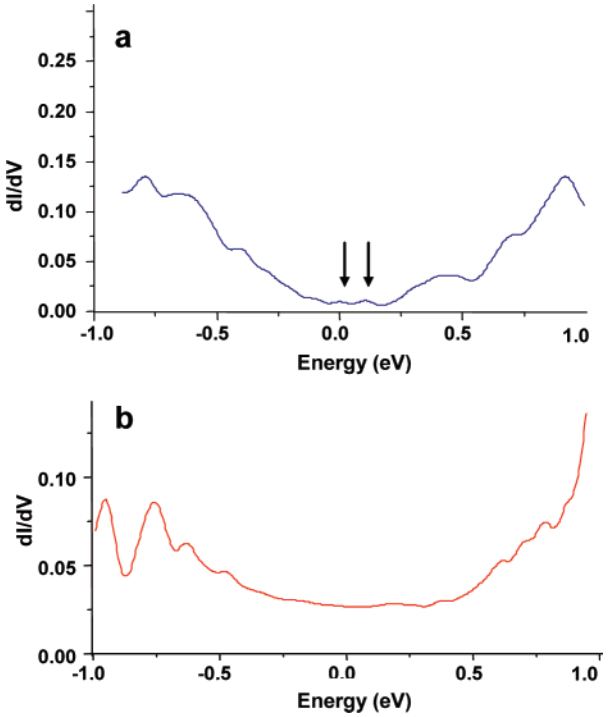

Figure 9. STS d*I*/d*V* curves of Tyr-nano-1-coated SWNTs on Au(111) show both (a) a vanishing DOS and (b) a nonvanishing DOS in the vicinity of the Fermi energy, suggesting that these two SWNTs coated with Tyr-nano-1 are electronically semiconducting and metallic, respectively. The black arrows in (a) point to weak peaks that appear on the conduction band side near the Fermi energy.

(Supporting Information). The STS curves taken at different positions along the uncoated region of the SWNT show consistent features. In contrast, the STS curves taken at different positions along the nano-1-coated region of the SWNT show variability in the VHS peak positions moving further away from the Fermi energy. These data suggest that the observed VHS fluctuations result from the interaction of the SWNT with the peptide rather than from experimental reasons, e.g., mechanical or electrical noise, tip contamination, or defects in the SWNT. Presumably, the peptide coating acts as a second barrier for electron tunneling which could cause a Coulomb blockade and staircase effect on the $I-V$ curves.[48,49,51] Similar charging effects have been reported for crossed carbon nanotubes[48] and cut nanotubes weakly coupled[51] and suspended from the surface.[49]

Since STS measurements of nano-1-coated SWNTs suggest a slight charge-transfer interaction between the SWNT and nano-1, we acquired STS spectra of nitro-nano-1/SWNT and Tyr-nano-1/SWNT dispersions to examine the effect of the nitro (electron-withdrawing) and hydroxyl (electron-donating) groups on the SWNT electronic properties. Figures 8 and 9 present a selection of STS d*I*/d*V* spectra of nitro-nano-1 and Tyr-nano-1-coated SWNTs, respectively. Figures 8a and 9a show d*I*/d*V* spectra with a pronounced dip in the DOS at the Fermi level, indicating that these peptide-coated SWNTs are electronically semiconducting. On the other hand, Figures 8b and 9b display d*I*/d*V* spectra with a nonzero DOS at the Fermi level, suggesting that these peptide-coated SWNTs are metallic. STS spectra were acquired from 11 nitro-nano-1-coated SWNTs in multiple sample preparations, for which 9 displayed semiconducting behavior and 2 exhibited metallic behavior, corresponding to 82% and 18% of the tubes investigated, respectively. STS spectra were acquired from 11 Tyr-nano-1-coated SWNTs in multiple sample preparations, for which 8 displayed semiconducting behavior and 3 exhibited metallic behavior, corresponding to 73% and 27% of the tubes investigated, respectively. The STS $I-V$ curves of 20 μM nitro-nano-1 and 100 μM Tyr-nano-1 control samples exhibit nonconducting behavior, and the respective d*I*/d*V* (DOS) spectra are featureless (Supporting Information).

Although the STS data demonstrate that these amphiphilic peptides do not severely disturb the SWNT electronic properties, there are some slight variations in the DOS of the peptide-coated SWNTs. The black arrow in the semiconducting d*I*/d*V* versus bias curve (Figure 8a) for a SWNT coated with nitro-nano-1 points to a weak feature and an increased DOS near the valence band side of the Fermi level. Likewise, the DOS of nano-1-coated portions of an individual SWNT revealed the appearance of weak features near the valence band side of the Fermi level (Figure 7b). These results are in contrast to the case of Tyr-nano-1-coated SWNTs where the semiconducting d*I*/d*V* versus bias curve appears to have weak features and an increased DOS near the conduction band side of the Fermi level (indicated by the black arrows in Figure 9a), whereas the valence band remains largely unaffected. We examined the peak positions for weak features found near the E_f (from -0.20 to 0.20 V) for all the SWNTs imaged, including the SWNT control and the three peptide/SWNT composites (Supporting Information). The weak features near the E_f are more prevalent in the d*I*/d*V* spectra

(51) Odom, T. W.; Huang, J.-L.; Kim, P.; Lieber, C. M. *J. Phys. Chem. B* **2000**, *104*, 2794−2809.

of the peptide-coated SWNTs than in the d*I*/d*V* spectra of the uncoated SWNTs. Only 27% of the d*I*/d*V* spectra for the SWNT control samples contained weak features found near the E_f compared to 72% of the d*I*/d*V* spectra for the peptide/coated SWNT samples. Additionally, to the best of our knowledge, these types of features have not been reported in the literature for HiPco SWNT DOS. The presence of new features at low bias voltages has been observed in tunneling spectroscopy of bent SWNTs.[27] The majority of the SWNTs imaged in the 100 μM nano-1/SWNT (78%) and 20 μM nitro-nano-1/SWNT (63%) dispersions exhibit weak features on the negative region or valence band side of the E_f. In contrast, the DOS of Tyr-nano-1-coated SWNTs have a predominance (72%) of weak features on the positive region or conduction band side of the E_f (Supporting Information). These results suggest that introducing an electron donor (hydroxyl) and an electron acceptor (nitro) on the benzene ring of Phe causes mostly an increased DOS on the conductance and valence band side of the Fermi level, respectively.

Previous STS studies of SWNTs intercalated with B and N atoms demonstrated that B-doped SWNTs exhibited prominent electronic acceptor states in the valence band,[5] whereas N-doped SWNTs had strong electronic donor states in the conduction band.[12] These additional features have been attributed to evidence of a doping or charge-transfer interaction. The electron acceptor and donor strength of the peptides are relatively much weaker owing to the nature of the noncovalent interaction between tubes and adsorbed peptide. It also follows that the electron donor feature observed in the spectra of 100 μM Tyr-nano-1/SWNT and the electron acceptor feature observed in the spectra of 20 μM nitro-nano-1/SWNT are not always present. Accordingly, it is possible that these small features near the E_f are the result of weak electrostatic (dipole−dipole and dipole−induced-dipole) interactions caused by π-stacking between the phenyl ring in the peptide and the graphene lattice of the SWNT. These types of interactions are intermittent and, at a given instant, are presumably present in only certain locations along the SWNT thus explaining why the weak features observed near the E_f are not always present.

Conclusion

In summary, we designed and synthesized peptides based on the nano-1 sequence in which the amount of electron density within the aromatic residue was systematically varied. Specifically, electron density was altered through the introduction of an electron-donating (hydroxyl) and an electron-withdrawing (nitro) group on the benzene ring by substituting the Phe residues in the nano-1 sequence with tyrosine and *p*-nitro-phenylalanine, respectively. CD was utilized to determine concentrations at which the peptides displayed an analogous secondary structure, both alone and in the presence of SWNTs, in order to allow us to examine the effect of the electron-donating/withdrawing character on peptide/SWNT interactions in the absence of secondary structure effects. AFM measurements and optical absorption spectra revealed that the ability to disperse individual SWNTs increases with increasing electron density of the aromatic residue on the hydrophobic face of the amphiphilic helical peptides.

Raman and STS were used to probe the peptide's impact on the electronic structure of the SWNTs. STM images showed that the peptides efficiently or fully coat the SWNTs. STS d*I*/d*V* spectra of the three peptide/SWNT dispersions displayed VHS peaks, characteristic of 1D SWNTs, and exhibited both vanishing and nonvanishing density of states around the E_f, suggesting that the peptide-coated SWNTs can exhibit both semiconducting and metallic behavior. STS d*I*/d*V* spectra of nano-1-coated portions of a SWNT closely resembled that of uncoated regions on the same SWNT with some slight modifications. Specifically, weak features that appeared on the valence band side near the E_f of the peptide-coated portion of a SWNT, as well as a shift of the Raman G band peak to higher frequencies for the nano-1/SWNT composite, are suggestive of a weak charge-transfer interaction in which nano-1 acts as an electron acceptor and the SWNT acts as an electron donor. Likewise, Raman and STS analyses suggest a very weak p-doping interaction between nitro-nano-1 and SWNTs. A small downshift of the Raman G band of the Tyr-nano-1/SWNT composite, compared to the nano-1/SWNT dispersion, as well as weak features on the conduction band side of E_f in the DOS of Tyr-nano-1-coated SWNTs, suggest a faint n-doping interaction between Tyr-nano-1 and the SWNT.

Altogether, these results suggest that the noncovalent peptide/SWNT interactions do not strongly perturb the electronic structure of SWNTs. In this context, designed peptides may provide an accessible means to incorporate the desired electrical properties of SWNTs into biocompatible nanoscale electronic devices. Microscopy results revealing that these peptides are capable of fully coating the SWNT surface and dispersing individual SWNTs will facilitate many applications of SWNTs to medical problems, such as artificial muscles or biomedical sensors that can be placed inside the human body. The amino acid sequence of these amphiphilic peptides could be further manipulated to promote the interaction of coated SWNTs with antibodies to peptide epitopes or to sense biological analytes designed to interact with the peptides.

Acknowledgment. The authors thank Professor Steven O. Nielsen for helpful discussions. The support of this research by the Robert A. Welch Foundation (AT-1326, I.H.M.), a Department of Homeland Security Fellowship (V.Z.P.), and a Young Investigator Grant from the Human Frontier Science Program (A.B.D., G.R.D.) is appreciatively acknowledged. This research was performed under an appointment to the Department of Homeland Security (DHS) Scholarship and Fellowship Program, administered by the Oak Ridge Institute for Science and Education (ORISE) through an interagency agreement between the U.S. Department of Energy (DOE) and DHS.

Supporting Information Available: Table of residues substituted in the *d* position of the nano-1 sequence, nitro-nano-1 UV−vis Beer's law standard calibration curve, STS d*I*/d*V* spectra taken at the same position on a SWNT control sample, CD spectra as a function peptide concentration, AFM images of peptide/SWNT and peptide control samples, AFM images and UV−vis−NIR absorption spectra of 100 μM nitro-nano-1/SWNT samples, STM images and STS d*I*/d*V* spectra of peptide control samples, STS spectra taken along the length of coated and uncoated regions of a nano-1-coated SWNT, and table of peak positions for weak features found near the E_f for all the SWNTs imaged, including the SWNT control and the three peptide/SWNT composites. This material is available free of charge via the Internet at http://pubs.acs.org.

JA0750827